6 Month Progress Report on

AIRCRAFT DIGITAL CONTROL DESIGN METHODS

Submitted to

NASA Langley Research Center

Hampton, Virginia

by

Michael G. Tashker
Information Science Laboratory
Stanford Research Institute

and
J. David Powell, Principal Investigator
Guidance and Control Laboratory
Stanford University

June 1975

Research Grant No. NSG-1137

Summary

The goals of the grant fall in two main areas. The first area is control system design and the goals are: 1) to define the limits of "digitized S-Plane design techniques" vs. sample rate, 2) to show the results of a "direct digital design technique" and 3) to compare the two methods. The second area is to evaluate the roughness of autopilot designs parametrically versus sample rate.

Goals of the first area have been addressed by 1) an analysis of a 2nd order example using both design methods, 2) a linear analysis of the complete 737 aircraft with an autoland obtained using the digitized S-plane technique, 3) linear analysis of a high frequency 737 approximateion with the autoland from a direct digital design technique, 4) development of a simulation for evaluation of the autopilots with disturbances and nonlinearities included.

An important aspect of the results to date is that the damping of the short period roots of the full 737/autoland system degrades by 50% at 5 cps (decreasing to 15% at 20 cps) with a slightly larger degradation of the dutch roll roots when using, in our judgement, the best digitized S-plane design technique.

Goals of the second area, roughness evaluation, have been addressed by defining an experiment to be carried out on the Langley motion simulator and coordinated with analysis at Stanford.

EXAMPLE: Pitch SAS - classical design

This system under consideration for the example is shown in Figure 1. The transfer function $\frac{\dot{\theta}(s)}{\delta e(s)}$ was derived for a 737 in cruise mode. The washout for pitch rate was chosen as being typical for a stability augmentation system. The washout break frequency, $1/\tau$, is chosen from the characteristics of the gyro bias and the expected nature of aircraft maneuvers producing a steady state pitch rate. For this system $\tau=1$ and $K=-.35$ yields roots of $-2.52 \pm 2.57\,j$ and $-.9865$. These will be considered the desired root locations for this example. The goal of a digital mechanization here will be to duplicate these roots.

Assuming a zero-order hold (Z.O.H.) signal reconstruction, the z-transform of the plant is:

$$\frac{\dot{\theta}(z)}{\delta e(z)} = .5275 \left\{ \frac{\left[e^{-1.4T}(\cos 3.28 - 3.24 \sin 3.28T) - 1\right] z + e^{-1.4T}(\cos 3.28T + 3.24 \sin 3.28T) - e^{-2.8T}}{z^2 - 2e^{-1.4T}\cos 3.28Tz + e^{-2.8T}} \right\}$$

where T is the sampling rate.

This is an exact result for the plant since there is a physical ZOH in the D/A conversion. There are, however, several possible mechanizations of the feedback washout. Methods under consideration and their results for the washout (including a constant to produce unity gain at high frequency) are:

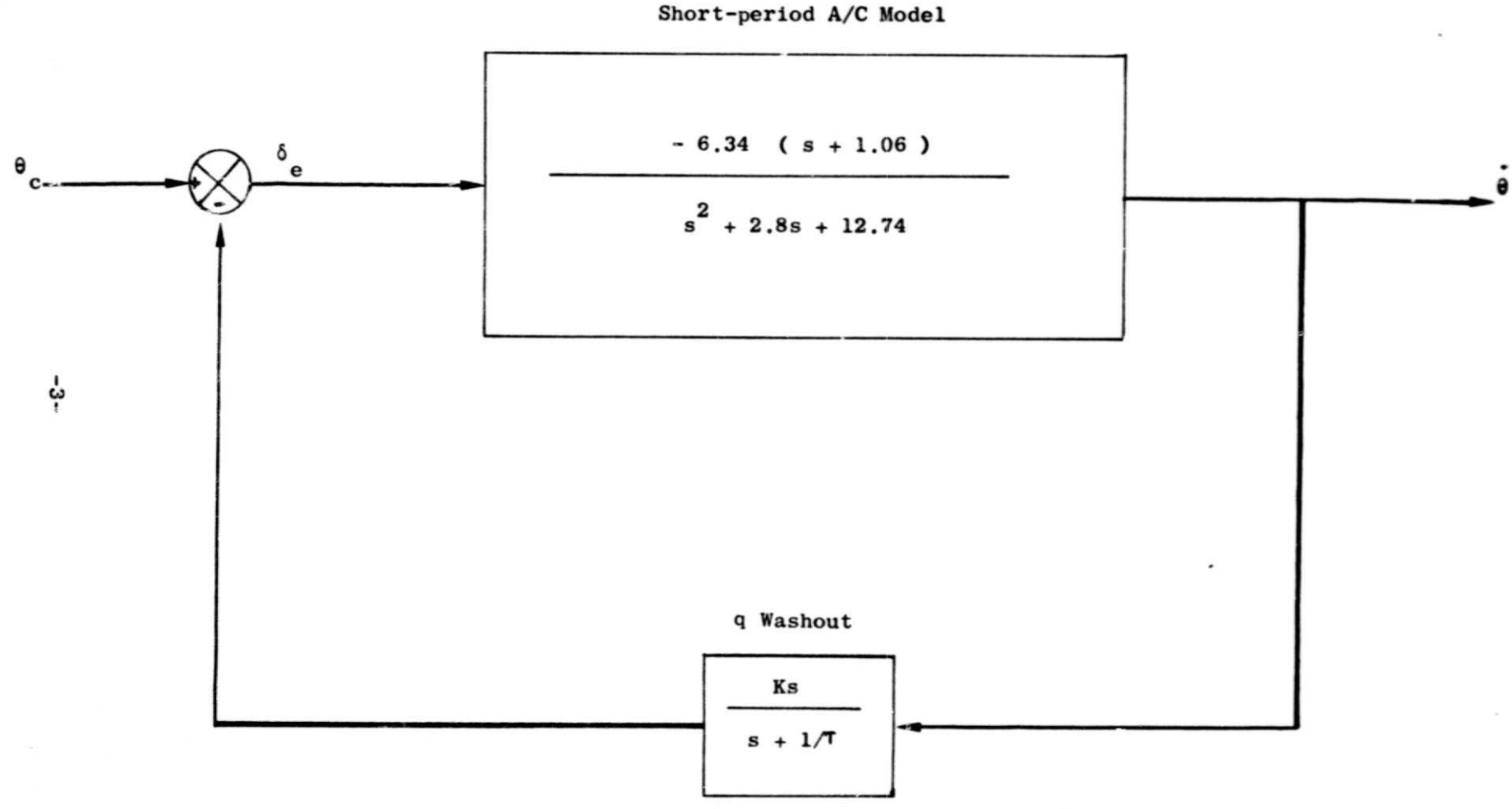

FIGURE 1 SHORT PERIOD MODEL

$$\frac{\frac{(1+e^{-T/\tau})}{2}(z-1)}{z-e^{-T/\tau}}$$; matched z-transform, Z.O.H., exact transform, Tustin with pre-warping

$$\frac{\frac{2}{2+T/\tau}(z-1)}{z-\frac{2-T/\tau}{2+T/\tau}}$$; Tustin

With the exception of Tustin's method (which also produces this result for high sampling rate) these methods produce the same transform, one that causes the pole and zero of the washout to be mapped into the z-plane by the transformation $z=e^{sT}$ for all sampling rates. This is inherently satisfying since the poles and zeroes are mapped exactly with no shifting at low sampling rates.

The z-transforms of the plant and the washout were used to study the variation in the roots of the sampled system as a function of sampling rate (shown in Figure 2). This variation comes from the change in position of the plant zero as a function of sampling rate. The feedback machanization has been chosen to produce no shift in poles or zeroes and examination of the denominator of $\frac{\dot{\theta}(z)}{\delta e(z)}$ reveals poles in the z-plane corresponding to the s-plane poles for all sampling rates. However the plant zero does not remain at -1.06 (the value for the continuous system), but shifts negatively as the sampling rate decreases (-1.1 for T=.2sec). This zero shift occurs for all plants with zeroes not at the origin. The variation in complex roots here tends to be more highly damped and the real root moves only slightly toward the origin. While this would seem to be an argument for

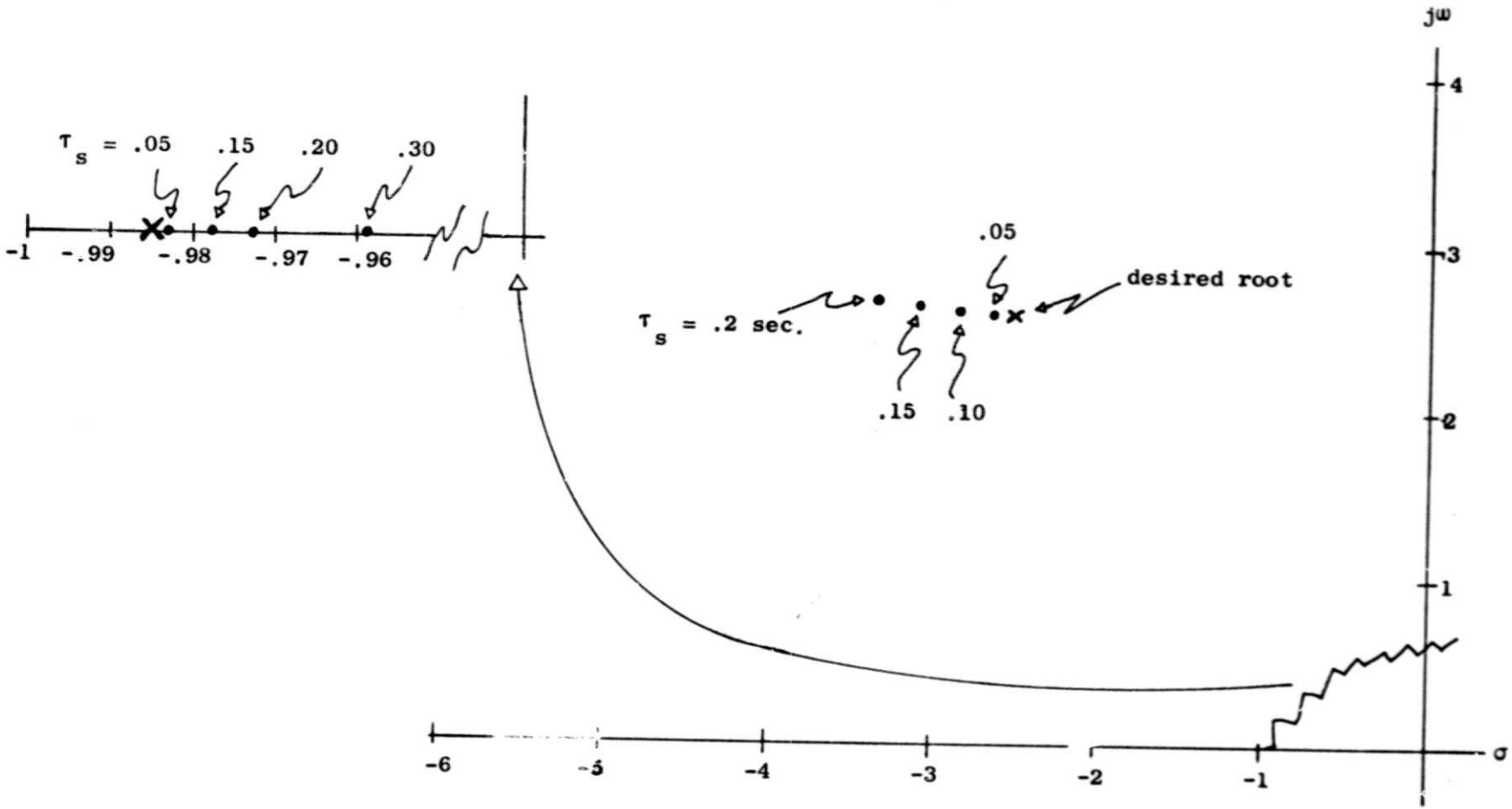

FIGURE 2 ROOT LOCATIONS FOR $\dot{\theta}$ FEEDBACK WITH WASHOUT

unconcern with slower sampling, this is not true for all situations (to be seen later in the 737 analysis).

This variation was generated with K and τ being the constant values resulting from continuous analysis. If they are allowed to vary as a function of sampling rate a system is produced that minimizes the distances between the roots and the desired roots, $d=\sum\left|r_i-r_{i_{desired}}\right|$. Figure 3 shows d for both the constant and variable gain cases, and the ratio of gains for the two cases. Variation of τ did not cause any decrease in d. Varying K yielded a maximum of 40 percent improvement in d over the constant gain case at 7 samples/sec.

The nature of the variation can be studied approximately by the following method: A root locus is drawn for the continuous system and the closed loop poles noted. The variation of the plant zero with sample rate can be computed explicitly from the expression of its z-transform. A family of loci may be sketched for different plant zero locations in the s-plane and the nature of the change in feedback may be explored. An exact analysis would require z-plane root loci; however, this method gives the same trends. For this example, the sketch (not to scale) would be as in Figure 4.

The relative invariance of the real root can be seen as well as the movement in the complex closed loop poles shown in Figure 1. Reducing the magnitude of K as indicated in Figure 3 will tend to move the poles along the dotted lines toward the open loop poles and consequently toward the desired root location.

It can be argued that the complex roots should be matched only,

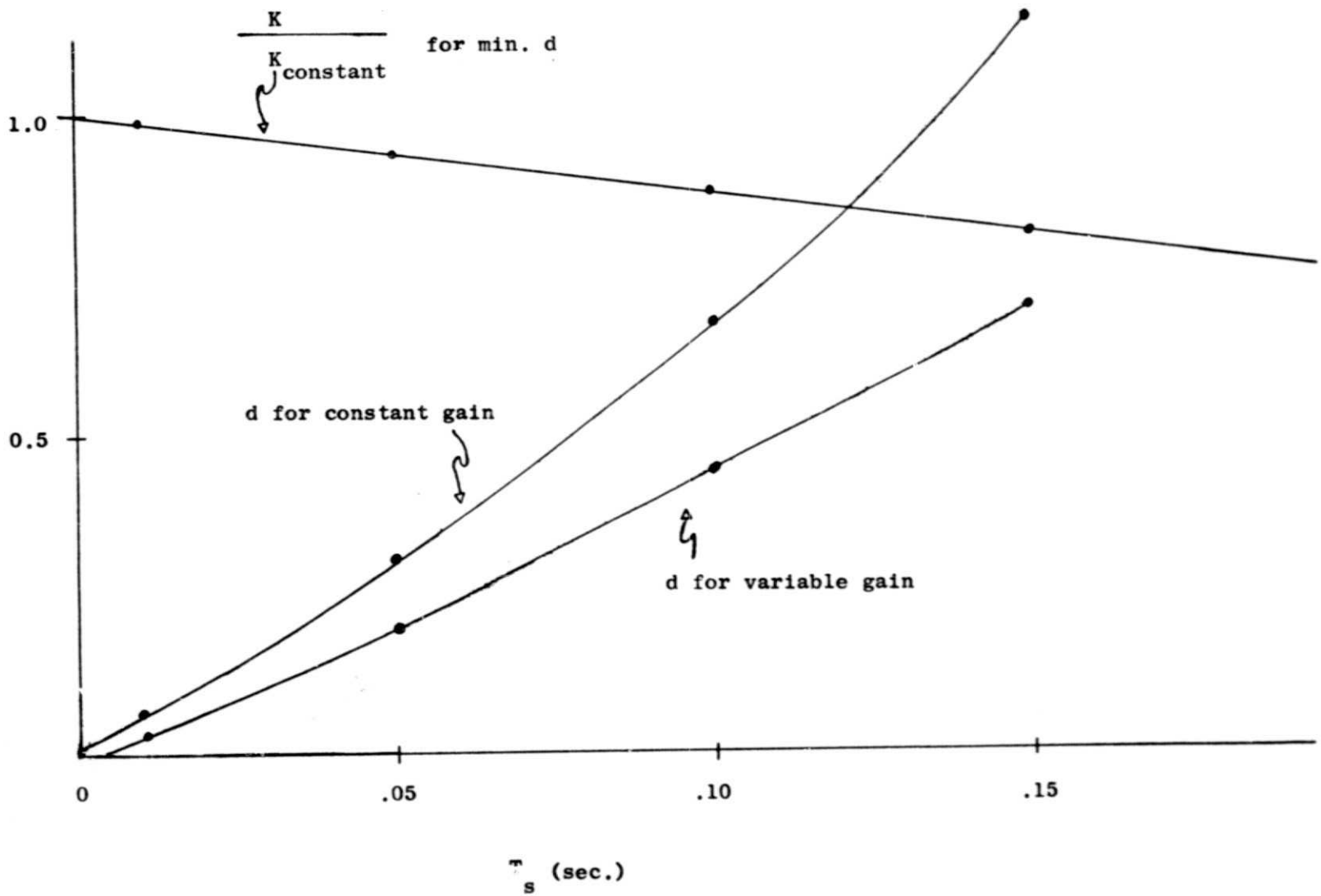

FIGURE 3 VARIATION IN ROOT DISTANCE AND GAIN AS A FUNCTION OF SAMPLING RATE

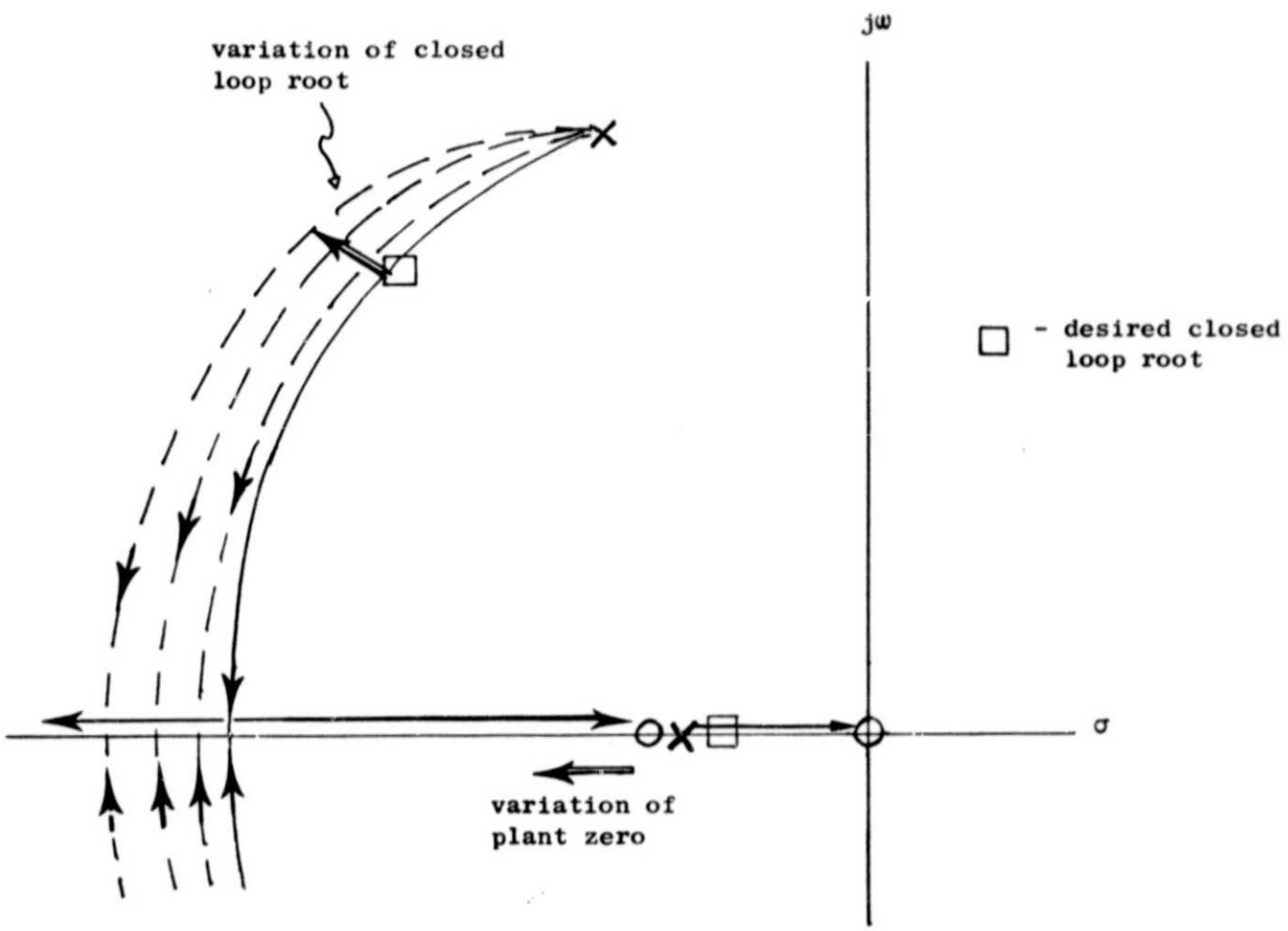

FIGURE 4 VARIATION OF CLOSED LOOP ROOTS AS A FUNCTION OF SAMPLING RATE (NOT TO SCALE)

leaving the real root (which is often at high frequency or relatively insensitive to changes) free.

There are two variables, K and τ, in the characteristic equation and therefore they should be sufficient to specify two roots. This is invalid however. If the two complex roots are $s=-R_1 \pm I_1 j$ and the real root is $s=-R_2$, the characteristic equation is

$$s^3 + (2R_1+R_2)s^2 + (R_1^2+I_1^2+2R_1R_2)s + R_2(R_1^2+I_1^2) = 0$$

The characteristic equation as a function of K and τ is of the form

$$s^3 + f_1(K,\tau)s^2 + f_2(K,\tau)s + f_3(K,\tau) = 0$$

and it can be seen by examining the dependence of R_1 and I_1 on f_1, f_2, and f_3 that in general K and τ cannot be varied so as to keep R_1 and I_1 constant.

In conclusion, the relatively simple procedure of changing feedback gains as a function of sampling rate will not retain the desired closed loop roots although some improvement is possible. It is also not possible in general to match some roots, leaving the others free. The reason that changes are occuring in the roots for slower sample rates is that an additional lag is being introduced into the system. To negate the effect of this lag, sophistication over and above simple gain changes is required to restore the system to its original performance.

EXAMPLE: State-Space Design

Another feedback technique is the design of an estimator and the use of estimated states in a control law. The state-space equivalent to the washout is a bias estimator for the steady-state component in q. Figure 5 shows the block diagram for such a system. There are two basic mechanization choices for an estimator: full state and reduced state. In this application it is natural to choose a reduced state estimator.

The state-space representation of the system with states q and α is:

$$\begin{bmatrix} \dot{q} \\ \dot{\alpha} \end{bmatrix} = \overbrace{\begin{bmatrix} -1.45 & -11.167 \\ 0.965 & -1.35 \end{bmatrix}}^{F} \begin{bmatrix} q \\ \alpha \end{bmatrix} + \overbrace{\begin{bmatrix} -6.34 \\ -.16 \end{bmatrix}}^{G} \delta e$$

Computing the matrices $\varphi = e^{FT}$ and $\Gamma = \int_0^T e^{Ft} G dt$ the discrete system is

$$x_{n+1} = \varphi x_n + \Gamma u_n$$

with the bias equation

$$b_{n+1} = b_n$$

Ignoring δe for the moment, a reduced state estimator can be built resulting in

$$\frac{\hat{q}(z)}{y(z)} = \frac{(1-L_2)(z-1)\left[z-\varphi_{22}+\frac{L_1\varphi_{12}}{1-L_2}\right]}{z^2+\left[L_1\varphi_{12}-1+L_2(1-\varphi_{11})-\varphi_{22}\right]z+L_2(\varphi_{11}\varphi_{22}-\varphi_{12}-\varphi_{12}\varphi_{21})+\varphi_{22}(1-L_2)-L_1\varphi_{12}}$$

for gains L_1 and L_2.

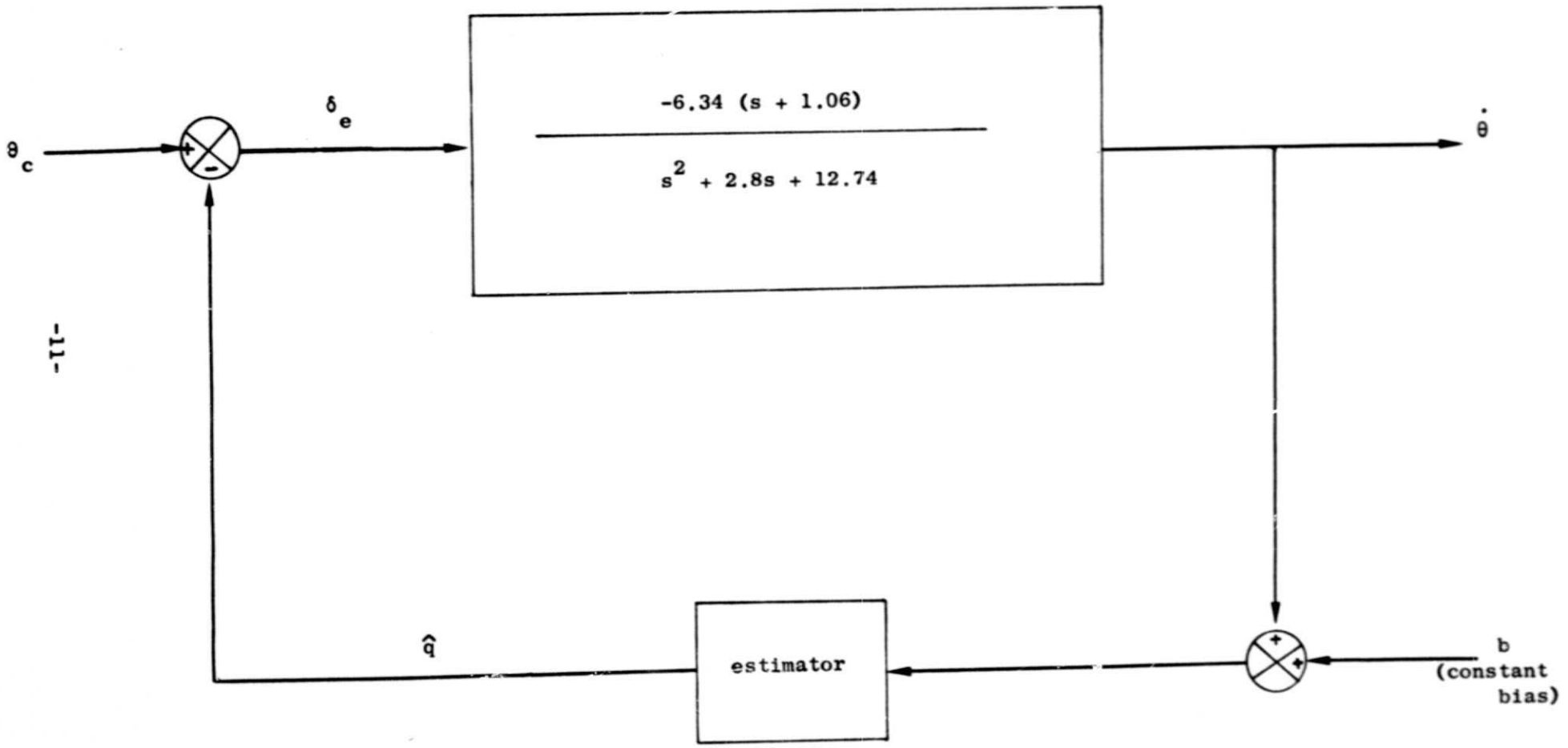

FIGURE 5 STATE SPACE MODEL

Comparing this to the digital washout where

$$\frac{\hat{q}(z)}{y(z)} = \frac{\left[\frac{1+e^{-T/\tau}}{2}\right][z-1]}{z-e^{-T/\tau}}$$

the estimator transfer function contains another pole and zero. There are only two gains and therefore the locations of the zero and both poles are not independent. While an estimator adds flexibility in choosing pole locations, it also adds a zero whose location is determined by the poles. In most modern control designs the zeroes between the observations and the estimated states are generally not taken into account because they do not appear in the transfer function between the commanded and actual output. But they do appear in the transfer function between the bias and the output. Thus their position is more important here and due to the lack of flexibility in placing the zero, it may be difficult to use this technique for sample rate compensation.

Discrete Control Laws

The continuous control laws for the 737 autopilot in the autoland mode prior to flare have been digitized using the "matched z-transform"[1] technique. As discussed in the example, the technique is almost identical to the prewarped tustin; however, it gives a better approximation when there are zeroes. For the transfer functions contained in the 737 autopilot, the digitized versions are:

$$\frac{K_c}{s+a} \longrightarrow \frac{K_D}{z+e^{at}} \quad ; \; K_D \text{ picked to match low frequency gain}$$

$$\frac{K_c S}{s+a} \longrightarrow \frac{K_D(z-1)}{z+e^{at}} \quad ; \; K_D \text{ picked to match hi frequency gain.}$$

$$\frac{1}{s} \longrightarrow \frac{z+1}{z-1}$$

The autopilot used in the digitization is shown in Figures 6, 7, 8 and represent our interpretation of the actual autoland autopilot. The aircraft linear model for the 2.5° approach configuration has been supplied by Langley and was used as is. Our interpretation of the auxilary equations relating the autopilot output to the aircraft input is shown in Fig. 9.

The effect of these digitizations were examined by a discrete linear analysis of the entire system composed of the autopilot, aux. equs and a/c model. Since there is negligible coupling between the longitudinal and lateral motion, the analysis was performed separately in the two axes. The z-plane roots resulting from this analysis were then transformed back to the s-plane by the transformation $s = \frac{\ln z}{T}$ so that they could be compared on an equivalent basis.

For the longitudinal system the continuous system (equivalent to infinitely small sampling interval) has the pole locations shown in Figure 10. As the sampling rate decreases the only roots that move appreciably are those associated with the short period mode (Figure 11). A system with a short period plant model, $\dot{\theta}$ feedback with a washout, and an actuator lag model produces the family of loci of Figure 12 vs. movement of the plant zero. These loci are relevant because, as was discussed in the example, the plant zero movement is a primary effect of discrete control. The direction of the movement corresponds well to the change in short period roots experienced by the entire longitudinal system.

The difference between this and the example considered earlier is the inclusion of the actuator lag (and the fact that the open loop roots are different). Here however the direction of movement of the short period poles is approximately perpendicular to the loci, and little improvement in pole position will be derived from decreasing the gain based on discrete analysis as in the example. Using this high frequency approximation, modifications to the discrete washout have been examined that increase the short period root damping back to the desired location for the slower sampling rates. The modifications consist of the addition of a pole and zero to increase the compensation lead so as to make up for the lag due to the sampler. At a 5 cps sample rate with short period closed loop roots at 1 cps, we do not anticipate any significant noise or disturbance amplification due to the increased compensation lead.

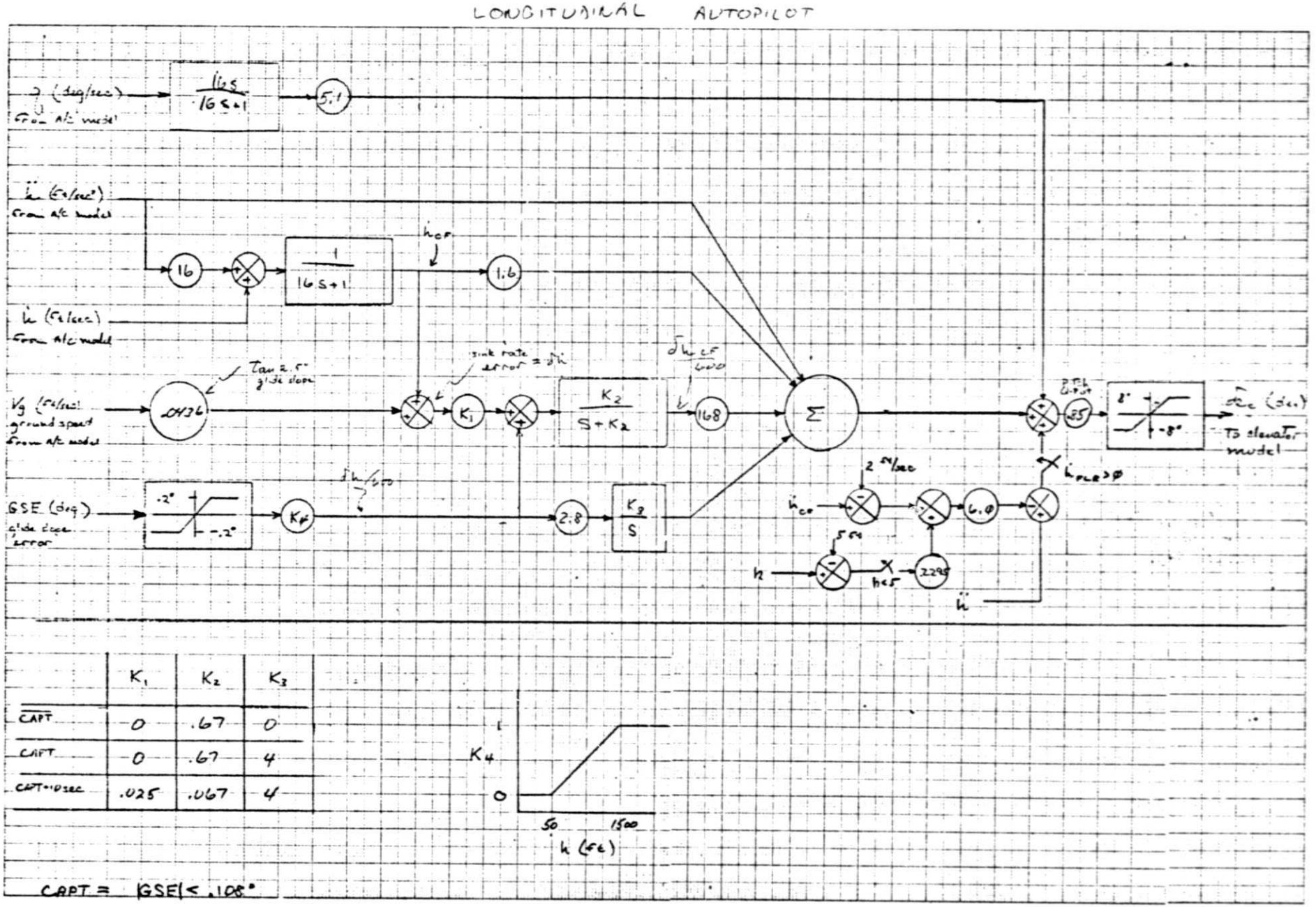

	K_1	K_2	K_3
CAPT	0	.67	0
CAPT	0	.67	4
CAPT+1Dsec	.025	.067	4

FIGURE 6

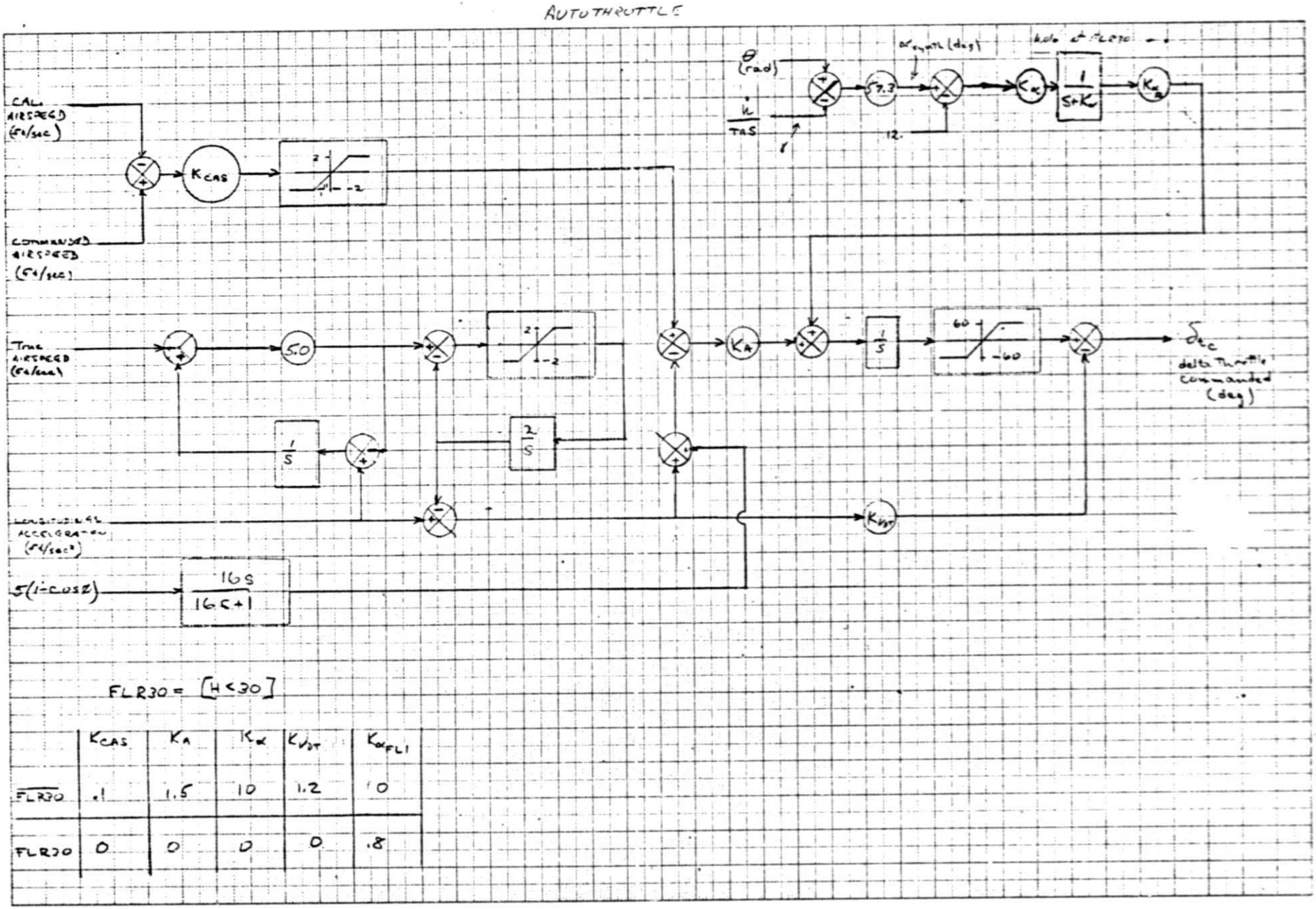

	K_{CAS}	K_A	K_α	$K_{V_{DT}}$	$K_{\alpha_{FL1}}$
$\overline{FLR30}$	.1	1.5	10	1.2	10
FLR30	0	0	0	0	.8

FIGURE 7

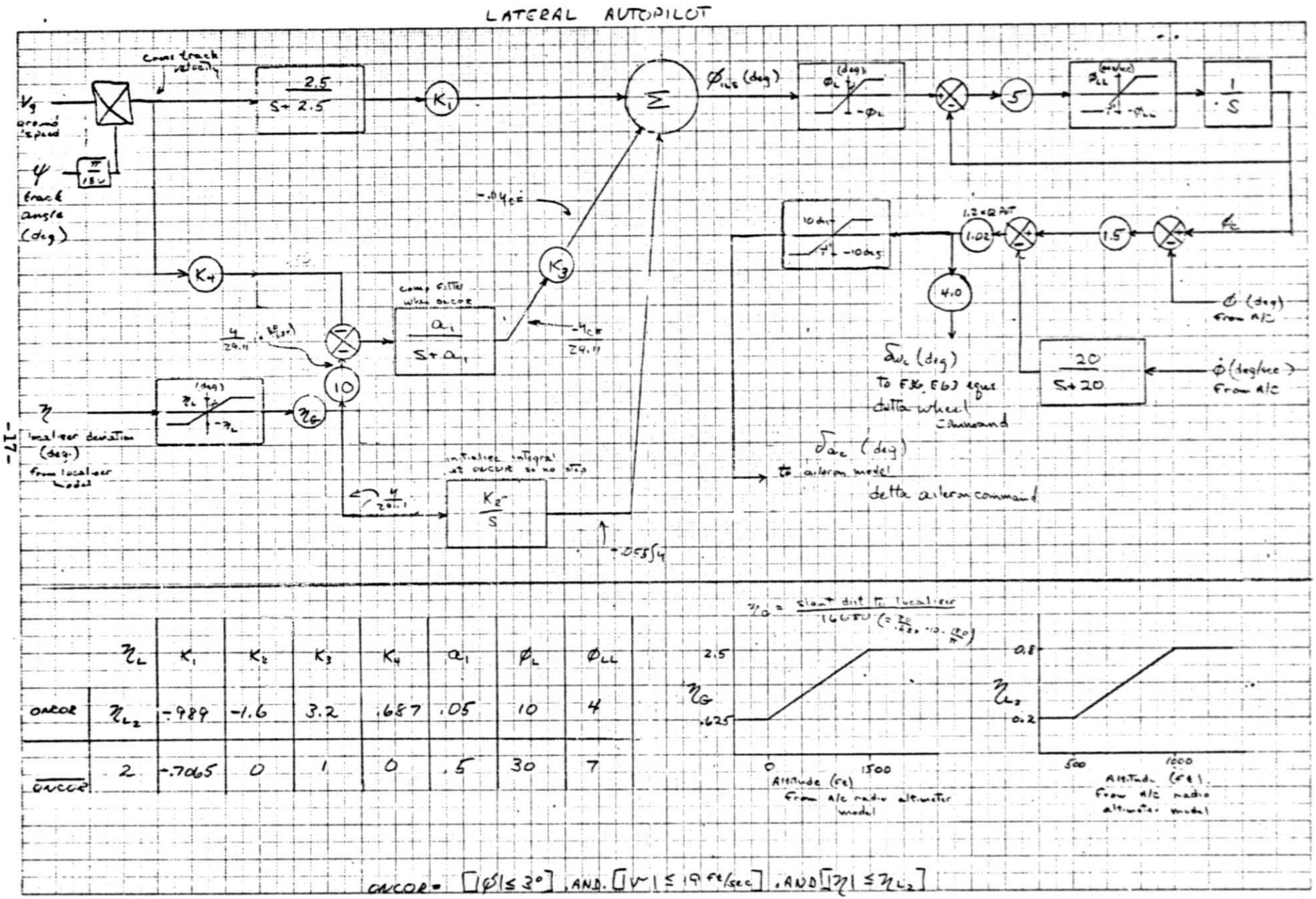

	η_L	K_1	K_2	K_3	K_4	a_1	ϕ_L	ϕ_{LL}
ONCOR	η_{L_2}	-.989	-1.6	3.2	.687	.05	10	4
$\overline{ONCOR}$	2	-.7065	0	1	0	.5	30	7

ONCOR = $[|\phi| \leq 3°]$ .AND. $[|V| \leq 19$ ft/sec$]$ .AND $[|\eta| \leq \eta_{L_2}]$

-17-

FIGURE 8

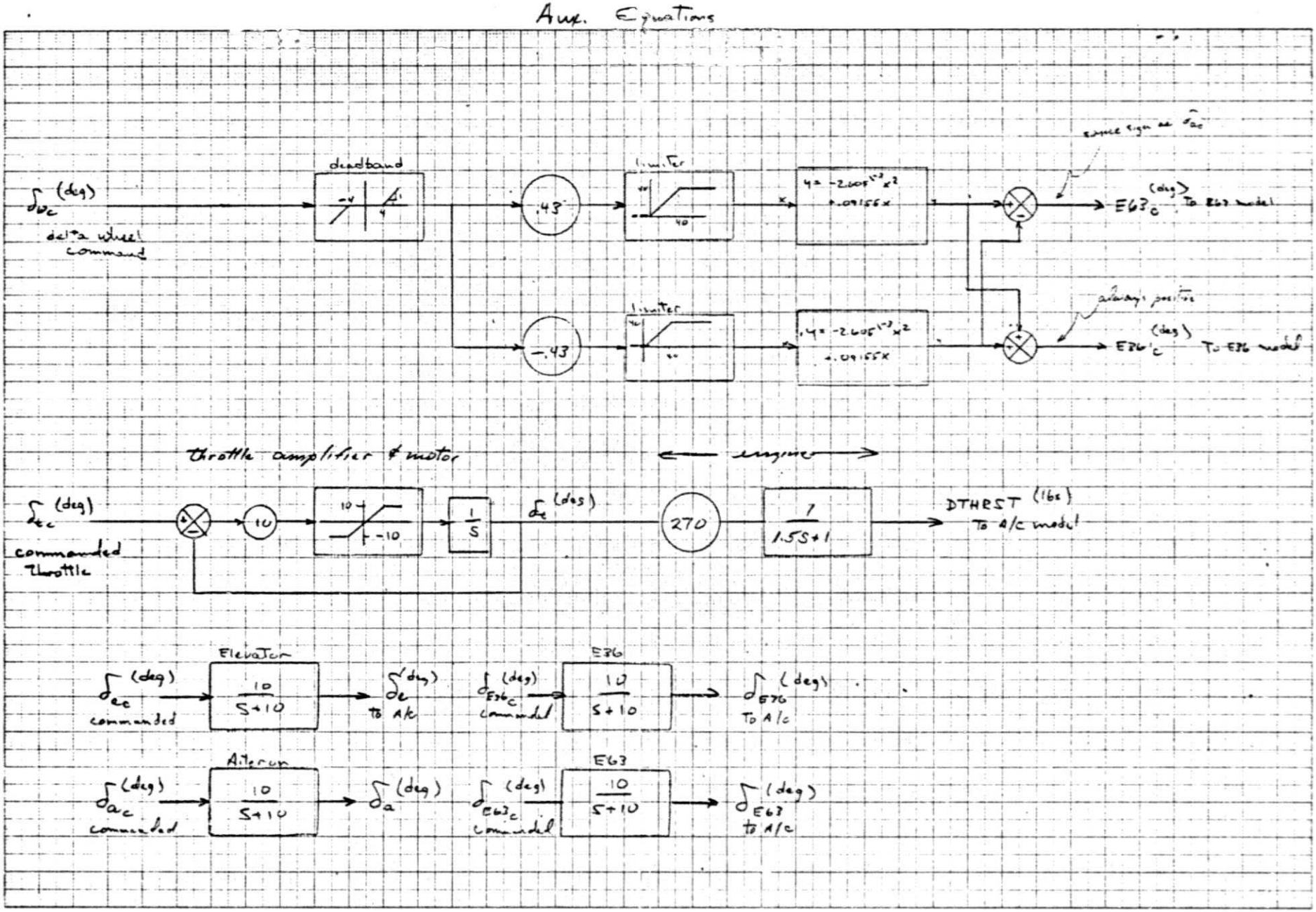
Aup. Equations
deadband
limiter
.43
-.43
same sign as δ_{wc}
always positive
$E63_c$ (deg) To E63 model
$E76_c$ (deg) To E76 model
δ_{wc} (deg)
delta wheel command
throttle amplifier & motor
engine
δ_{tc} (deg)
commanded Throttle
10
-10
1/S
δ_t (deg)
270
1/(1.5S+1)
DTHRST (lbs) To A/c model
Elevator
E76
Aileron
E63
10/(S+10)
δ_{ec} (deg) commanded
δ_e (deg) To A/c
δ_{E76_c} (deg) commanded
δ_{E76} (deg) To A/c
δ_{ac} (deg) commanded
δ_a (deg)
δ_{E63_c} (deg) commanded
δ_{E63} (deg) to A/c

FIGURE 9

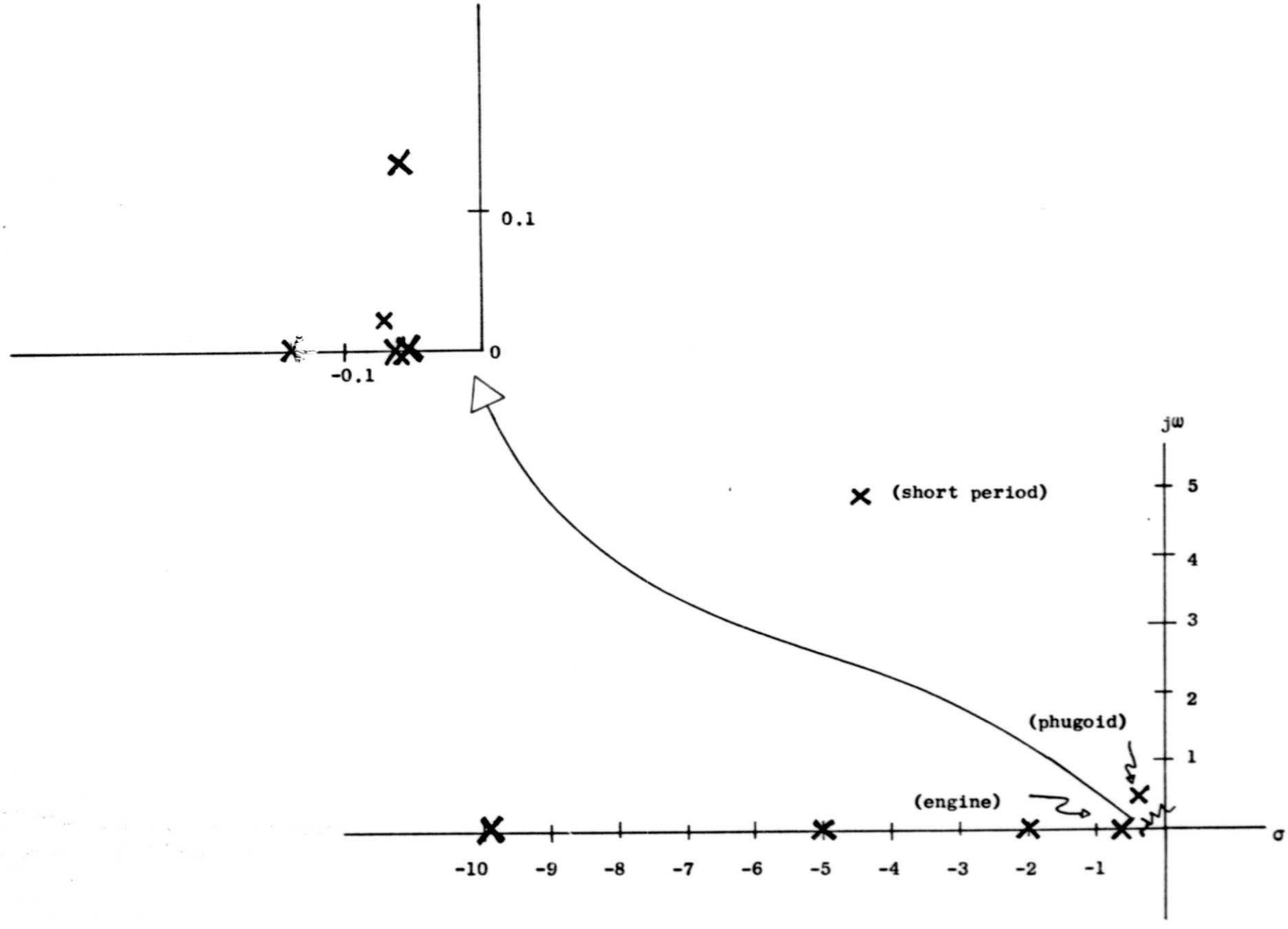

FIGURE 10 DESIRED CONTINUOUS LONGITUDINAL ROOT LOCATIONS

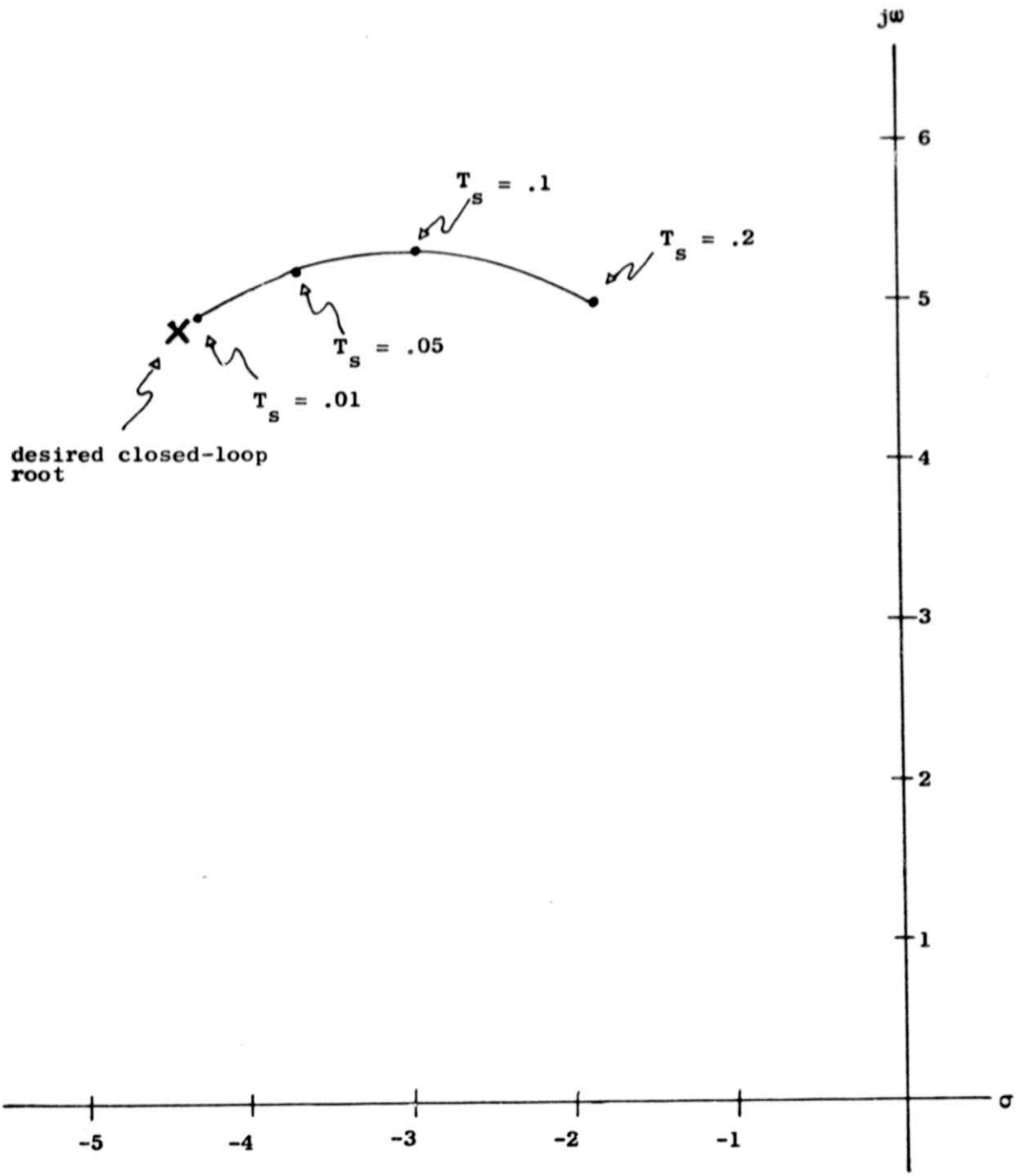

FIGURE 11 SHORT PERIOD ROOT LOCATION VS. SAMPLING RATE

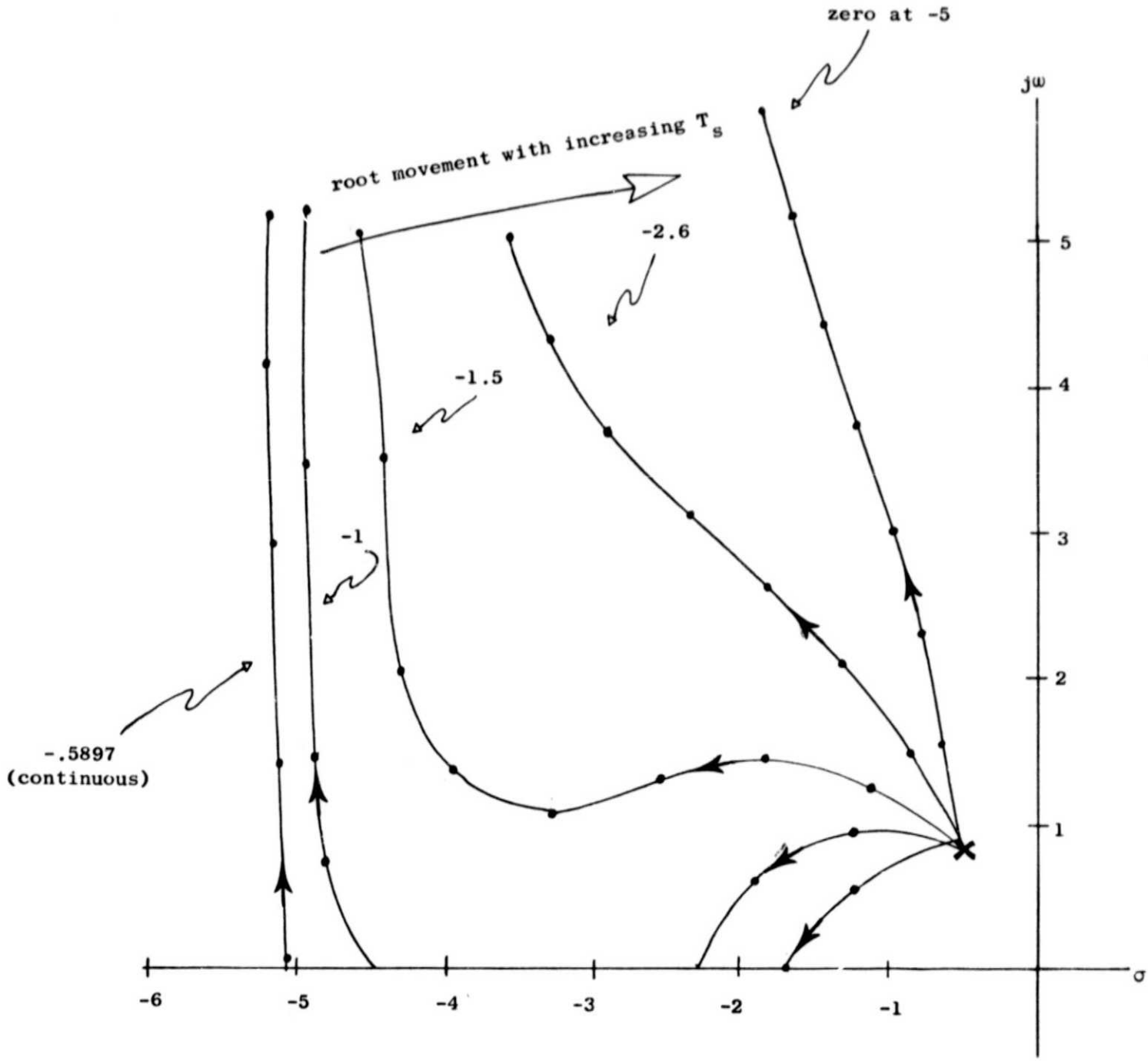

FIGURE 12 FAMILY OF LOCI OF SHORT PERIOD ROOTS VS. ZERO MOVEMENT

The desired lateral roots are shown in Figure 13 and the variation in these roots that change is shown in Figure 14. The roots that change are those associated with the $\frac{5}{s+5}$ loop on the lateral autopilot drawing (Figure 7) and the roll subsidence as well as the aileron lag and the dutch roll. The lateral system has not yet been analyzed to determine the critical feedback loop where additional compensation can be introduced in a direct digital design to reduce root movement. These results were obtained by a linearization that assumed the spoiler threshold was not exceeded. In obtaining the final digital designs, an additional linearization where the threshold is exceeded, thus approximating larger perturbations, will be used to evaluate the designs.

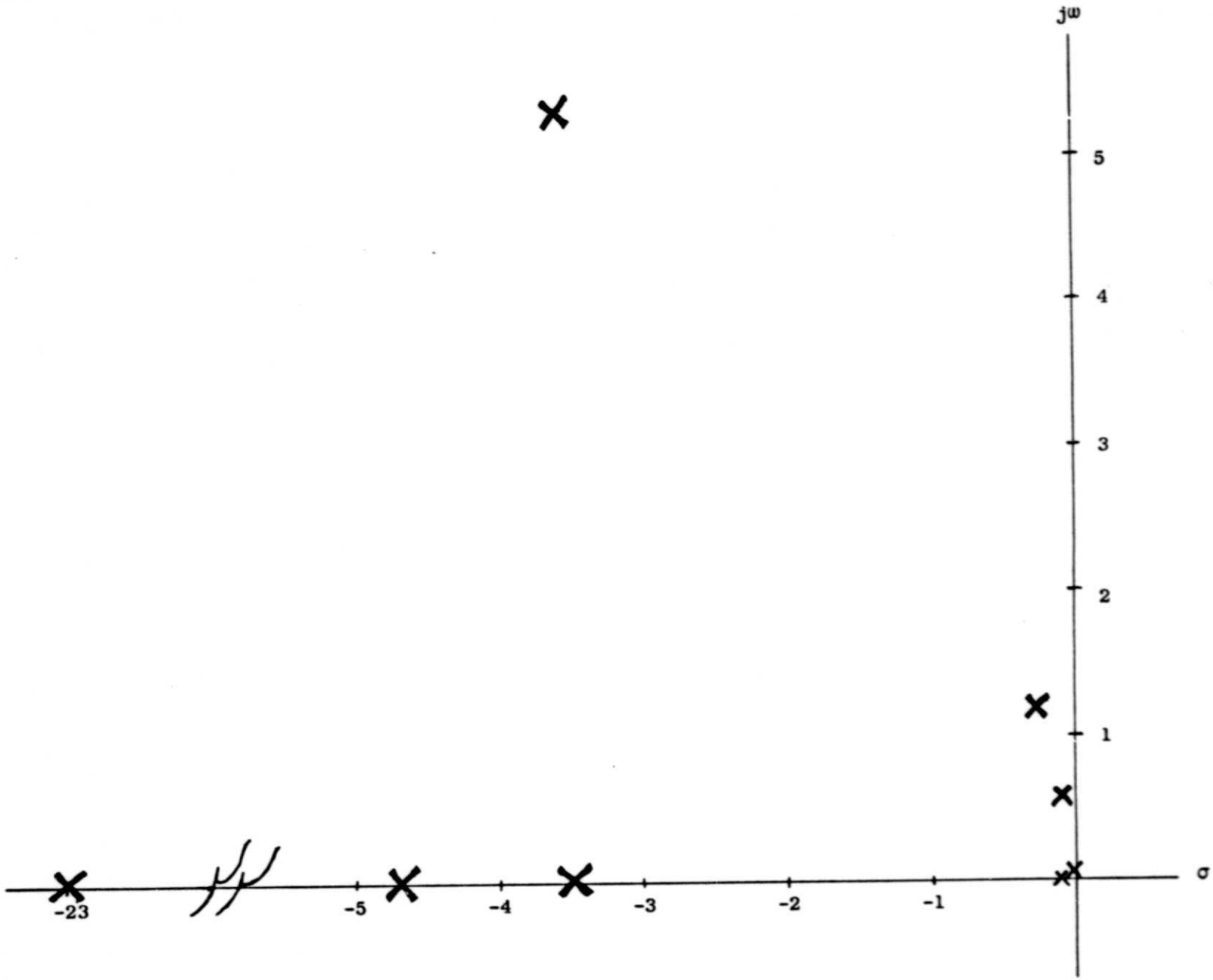

FIGURE 13 CONTINUOUS ROOTS OF THE LATERAL AUTOPILOT

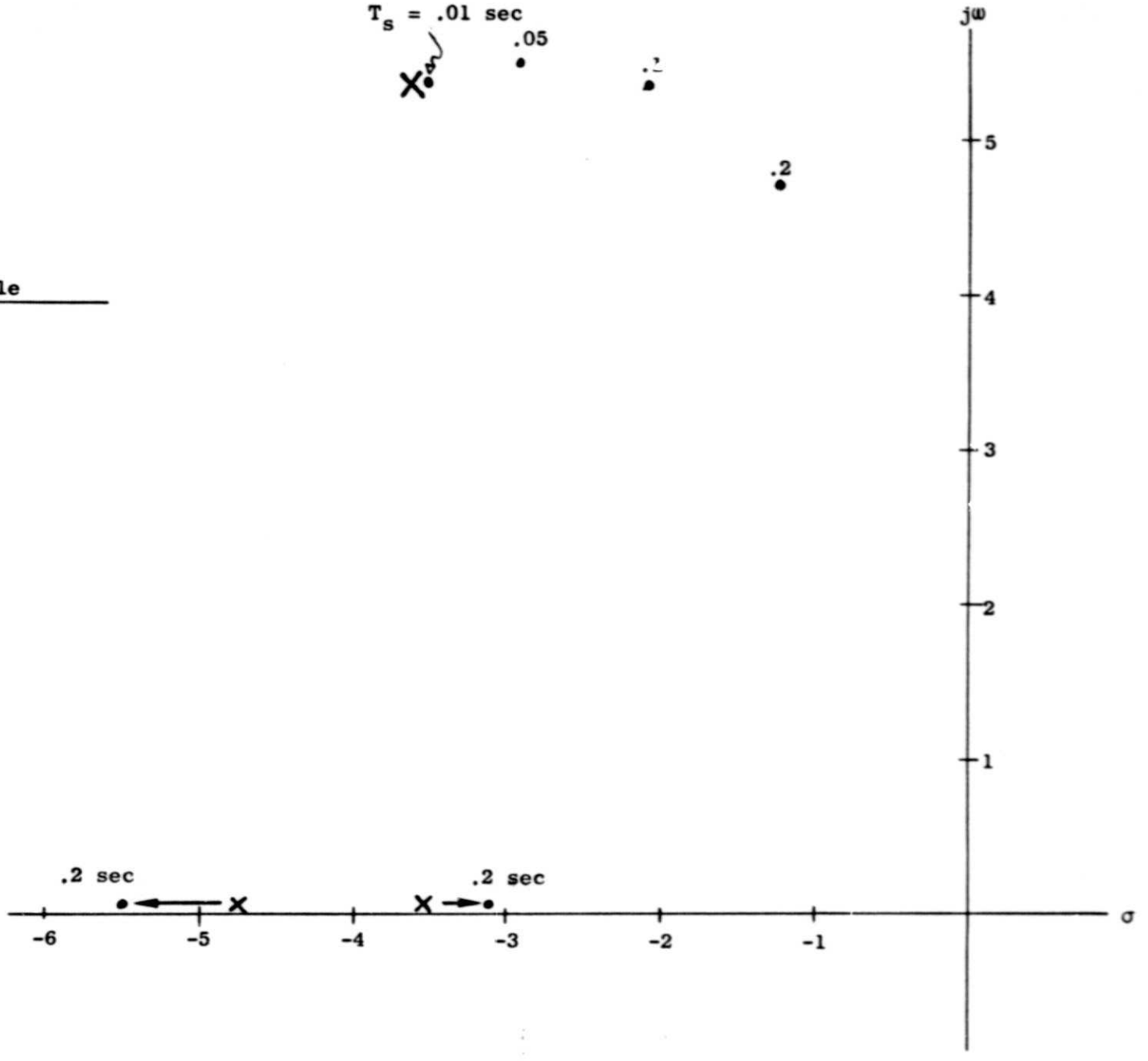

High Frequency Pole	
T_s	σ
0	-23.1
.01	-23.3
.05	-25.7
.1	-53.5
.2	-14.

FIGURE 14 LATERAL ROOT MOVEMENT VS. SAMPLING RATE

Autopilot/Aircraft Simulation

In order to verify the discrete control laws in a more complete fashion than is possible with a linear analysis, a simulation of the aircraft/autopilot has been coded. It will enable us to determine the effect of the various autopilot saturations and the spoiler deadband on the autopilot performance and will provide an independent verification of the designs. Furthermore, flight path time histories in the presence of wind gusts will be obtained to evaluate accuracy of the various designs.

The simulation is a Fortran program of the aircraft controlled by the autopilot. The aircraft dynamic equations are the linearized small perturbation equations for the glide slope configuration written in standard first order form:

$$\dot{x} = Ax + Bu + B'w$$

These are integrated by a fourth order Runga Kutta algorithm using an input initial state and time increment. The state vector expresses the vehicle's angular velocity and orientation, as well as its rectilinear motion, and position in a ground fixed reference frame. A general autopilot subroutine determines the control vector on the basis of the current state after a user-specified number of repetitions through the integration loop (effectively determining sampling rate).

An optional digital simulation of atmospheric turbulence is included and the effect of uniform gusts and gust distributions over the aircraft is modeled by B' in the equation above.

The gust vector w represents a disturbance to the system consisting of wind gusts (u_g, v_g, w_g) together with gust angular velocities (p_g, q_g, r_g). u_g, v_g, w_g, and p_g are uncorrelated turbulence components while q_g and r_g are related to $\frac{\delta w_g}{\delta x}$ and $\frac{\delta v_g}{\delta x}$ respectively. The six turbulence components have a normal magnitude distribution with zero mean and a variance related to the mean wind, a function of altitude.

The power spectral densities of the turbulence components are Dryden Spectra, which assume the longitudinal spatial autocorrelation function of gust velocity to be of the form

$$R(r) = \sigma^2 e^{-\frac{r}{L}}$$

Here, σ is the gust variance, and r is a general spatial coordinate. L, the characteristic scale length of the turbulence, is related in general to altitude.

The continuous domain power spectral densities implied above (2,3) are digitally recreated by passing a Gaussian random number sequence through appropriate difference equations (4).

The program is completely coded and in the final stages of checkout. Simulations have been made of an aircraft trajectory on a glide slope and found to give accurate results. Checkout of the system coupled to an autopilot and the wind model is now being checked out.

Roughness Evaluation

The results of the discrete linear analysis of the digitized s-plane designs show that the actuator plus short period aircraft dynamics give an accurate representation of the high frequency behavior of the full longitudinal dynamics. Furthermore, all significant root movement due to sample rate is exhibitied by this simplified mode. The intent of the roughness evaluation is to determine the effect of slow sampling in terms of response roughness or jerkiness as perceived by a pilot. These effects will be most noticeable in the high frequency modes of the aircraft. Therefore, the short period aircraft dynamics with the elevator lag has been selected for these studies.

To more fully evaluate pilot response the high frequency approximation to the autoland and the control wheel steering modes will be evaluated. The autoland mode essentially places the pilot in a monitoring type of function and may produce different reactions compared to the control wheel steering where he will be required to execute various tasks.

The holds to be considered are (Fig. 15) the standard zero order hold (ZOH) for a baseline, the first order hold, and the triangular hold. The first order hold essentially requires two outputs representing the step in the control, Δu in Fig. 16, and the slope, k_i. It shares the disadvantage of the ZOH that step changes in the control occur.

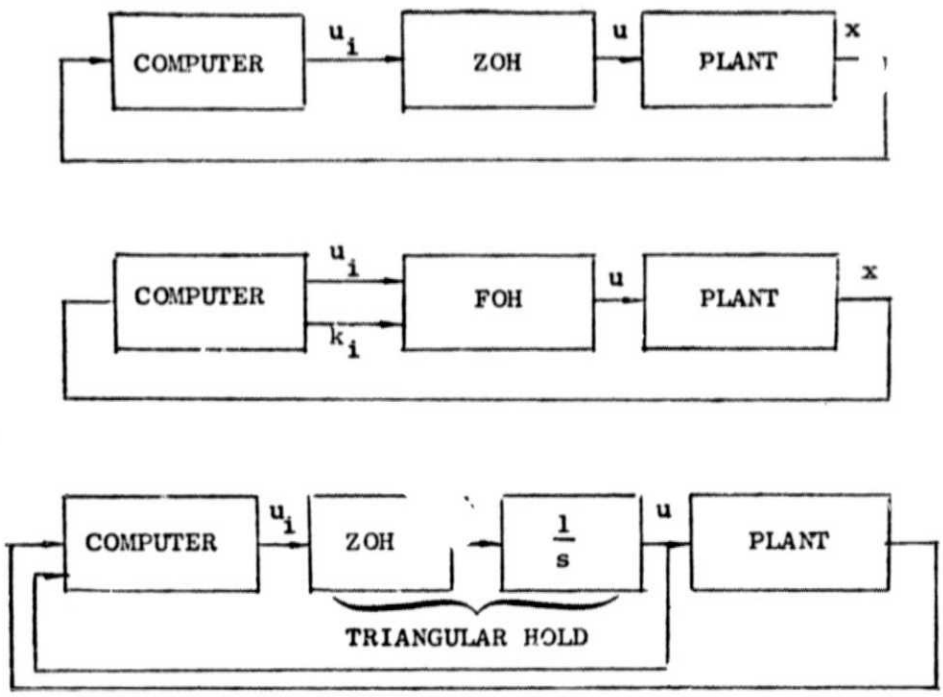

Figure 15

To eliminate this disadvantage, a triangular hold (TAH) is included which has the additional advantage of being particularly straightforward to mechanize, i.e. an integrator is placed between the ZOH and the actuator.

Figure 17 combines the different elements of the evaluation and indicates where the different portions of the computations are to be carried out. The aircraft model is given by:

$$\frac{q(s)}{\delta e(s)} = \frac{K(s+a)}{(s+b)(s^2+2\zeta\omega_n s+\omega_n^2)}$$

where b = actuator lag (10 r/sec)

K, a, ζ, ω_n = short period dynamics (dependent on flight condition)

$$\frac{\theta(s)}{q(s)} = \frac{1}{s}$$

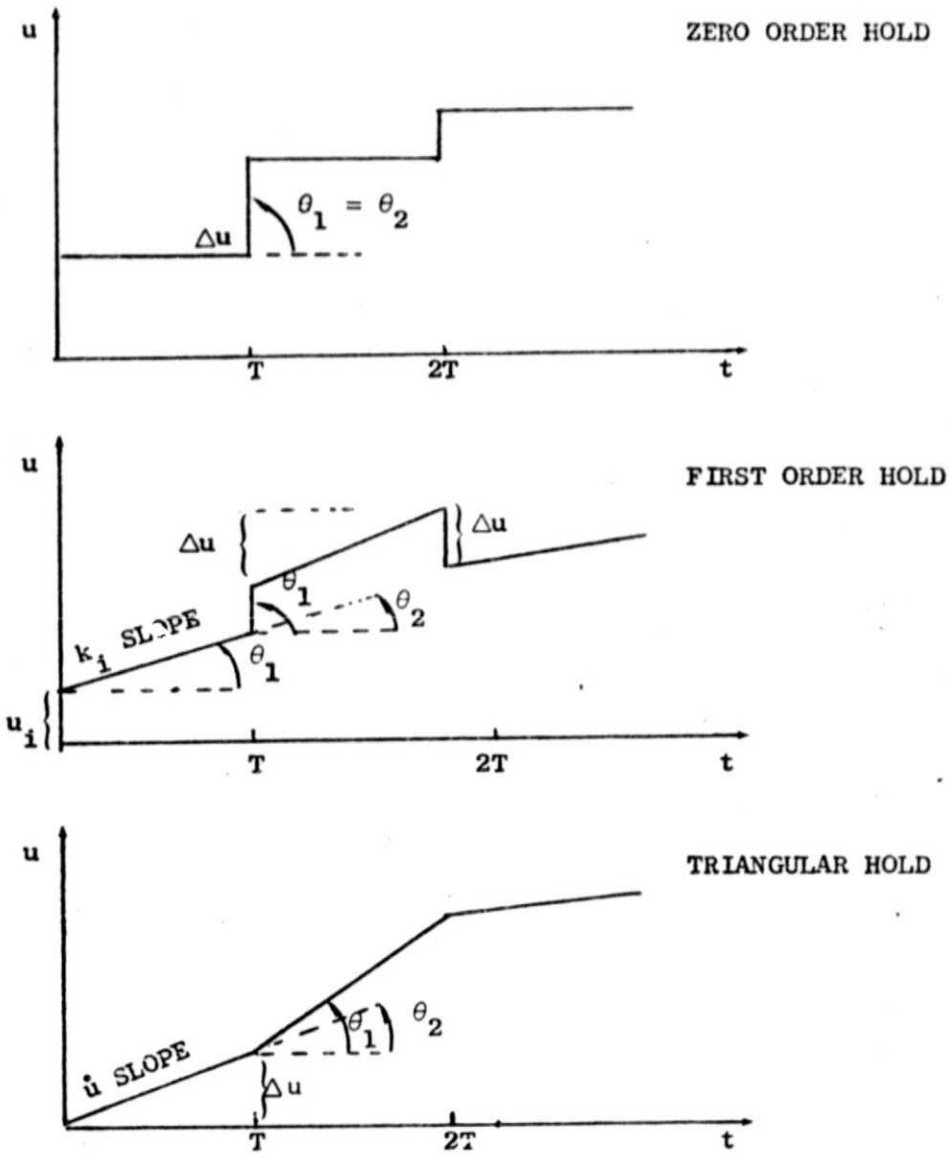
ZERO ORDER HOLD
u
Δu
θ1 = θ2
T
2T
t
FIRST ORDER HOLD
u
Δu
Δu
θ1
θ2
ki SLOPE
θ1
ui
T
2T
t
TRIANGULAR HOLD
u
θ1
θ2
u̇ SLOPE
Δu
T
2T
t

Figure 16

Analog Computers (EAI 231R's)

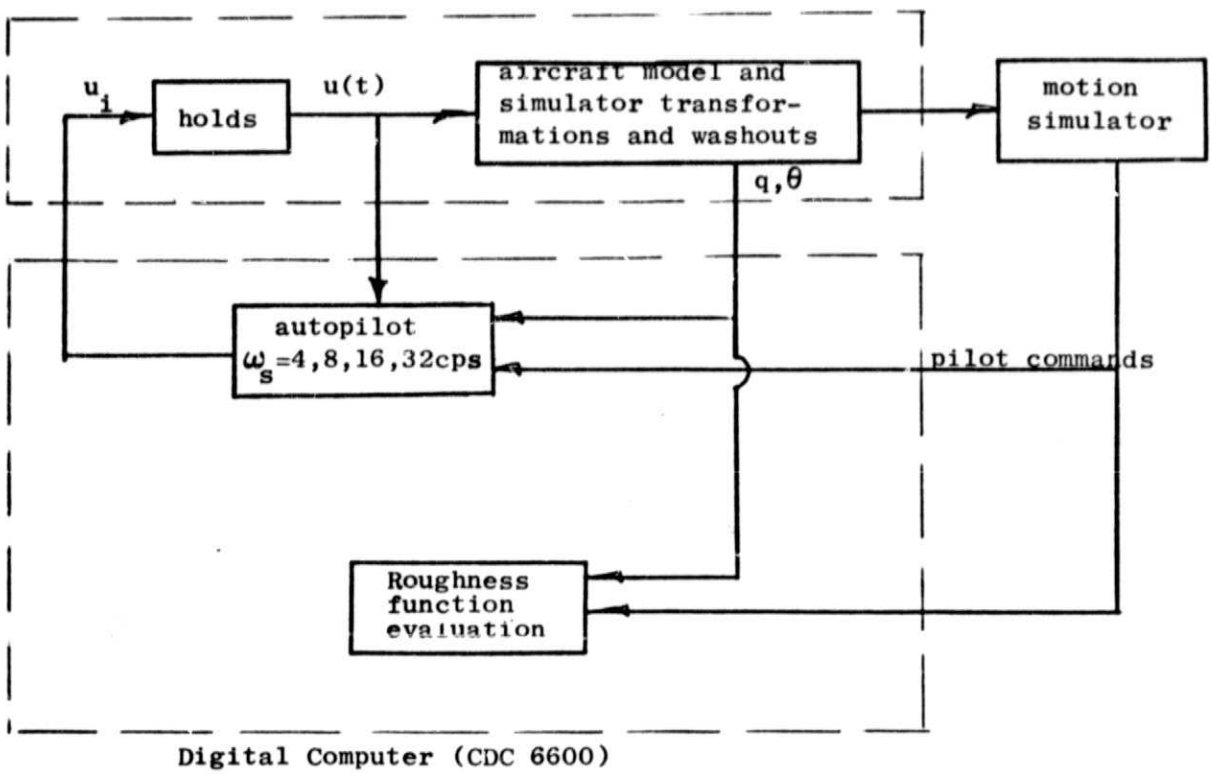

Figure 17

The algorithms to be implemented for the holds are:

ZOH: $u(t) = u_i ; t_i < t < t_i+1$

FOH: $u(t) = u_i + k_i(t-t_i); \quad t_i < t < t_{i+1}$

TAH: $u(t) = \int_o^t u_i dt$

The autopilot equations will basically be discretized versions of the pitch rate feedback through a washout (Fig. 6), proportional pitch attitude feedback, and the stick force input through a filter with associated control wheel steering logic. In addition, extra compensation for slow sampling will add one past value of measured states and one past value of control output for all holds. For the FOH, the control slope is required necessitating one additional difference equation:

$$k_i = \frac{u_i - u_{i-1}}{T}$$

For the TAH, the additional integration of the plant will require further compensation in the autopilot. To eliminate effects of drift, we anticipate the additional feedback of the integrated control will be useful.

Analytical evaluations of roughness have been proposed[5] and are:

$$RF_1 = \sum_{i=o}^{N} \left(\frac{\theta_1}{\pi/2}\right)^2 \Delta u^2$$

$$RF_2 = \sum_{i=o}^{N} \left(\frac{\theta_2}{\pi/2}\right)^2 \Delta u^2$$

$$RF_3 = \max\left|\frac{\theta_2}{\pi/2} \Delta u\right|$$

$$RF_4 = \max\left|\frac{\theta_1}{\pi/2} \Delta u\right| .$$

where the terms are defined in Fig. 16. These functions will be evaluated in the digital computer and correlated with the pilot evaluations of roughness.

The exact nature of the evaluations with regards to initial conditions for the autoland, test maneuvers for the control wheel steering, and form of pilot evaluations, will be determined in collaboration with Langley personnel.

Financial Status

Expenditures are slightly below projections and are indicated in Figure 18. Due to the higher Stanford expenditure rates through the summer months, we anticipate higher productivity through this period.

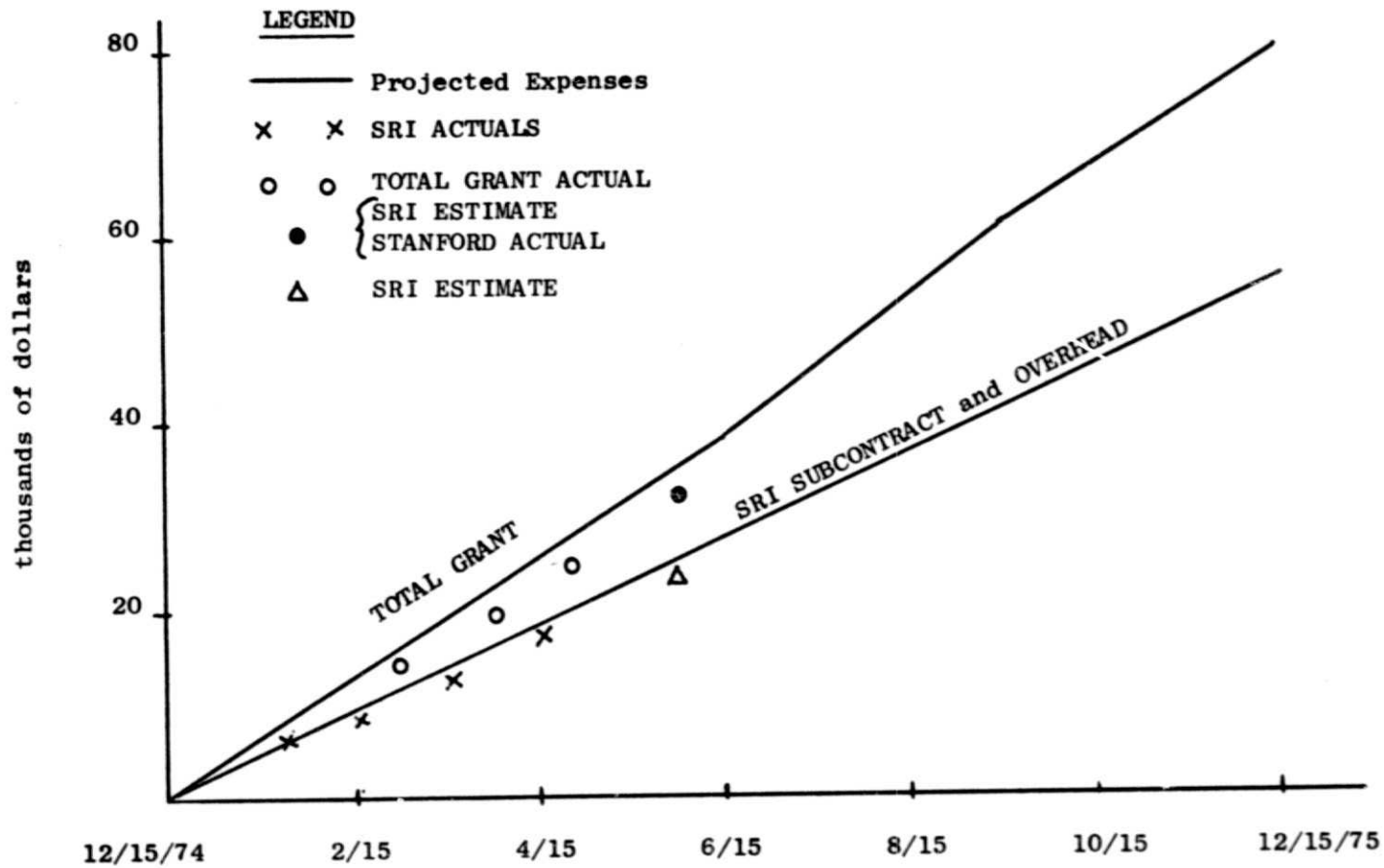

Figure 18

Actual and Projected Expenditures

References

1. G. L. Slater, A Unified Approach to Digital Flight Control Algorithms. AIAA paper No. 74-884 presented at Mechanics and Control Flight Conference, Anaheim, Calif. Aug. 1974.

2. Modeling Turbulence for Flight Simulation at NASA-Ames by Benton L. Parris, January 1975.

3. B. Etkin, Theory of Flight of Airplanes in Isotropic Turbulence -- Review and Extension, AGARD Report 372, 1961.

4. F. Neuman and G. D. Foster, Investigation of a Digital Automatic Aircraft Landing System in Turbulence, NASA TN D-6066, October, 1970

5. P. Katz and J. D. Powell, Selection of Sampling Rate for Digital Control of Aircraft, Sudaar Report No. 486, Sept. 1974